Journal of Engineering Mathematics (2006) 54: 119–143
DOI 10.1007/s10665-005-9007-0

A mathematical model for the use of a Gough-Stewart platform mechanism as a fixator

H. MUTLU, İ.D. AKÇALI[1] and M. GÜLŞEN[2]
Mechanical Engineering Department, University of Mersin, Mersin, 33160, Turkey; [1]*Mechanical Engineering Department, University of Çukurova, Adana, 01330, Turkey (E-mail: idakcali@mail.cu.edu.tr);*
[2]*Department of Orthopaedics and Traumatology, University of Çukurova, Adana, 01330, Turkey*

Received 19 May 2004; accepted in revised form 27 June 2005 / Published online: 16 November 2005

Abstract. One of the spatial external fixators, which can provide six degrees of freedom, three rotations and three translations, in handling extremity fractures and deformity-correction cases, is the so-called Gough-Stewart Platform Mechanism with six adjustable bars and two platforms. A mathematical model is developed for an effective deployment of the apparatus in orthopaedic processes. The model basically accepts input radiographic and clinical data and provides the bar lengths under several conditions and possibilities systematically studied, on the one hand, and predicts the behavior of the fixator assembly as to the guiding of the bone fragments in a controlled fashion determined by the treatment strategy, on the other. Numerical examples are presented to verify the model.

Key words: deformity correction, inverse and direct kinematics, medical application, radiographic and clinical data, rotation matrix

1. Introduction

In orthopaedic clinical practice, treatment of complex bone deformities and reduction of old, unreduced fractures are always problematic. Currently, circular fixators are used mainly to solve these problems because of their capability of six-degrees-of-freedom bone displacement, [1, pp. 287–543], [2, Chapter 12]. Gradual movement of the bone fragments not only provides safe correction but also promotes bone healing by distraction osteogenesis. In acute fractures, if the surgeon prefers to use a circular fixator, it is usually difficult to hold the reduction during the application of the frame, so some residual displacement occurs. Hinges, translation and rotation devices and rods are used for bone displacement. Very careful pre-operative planning and precise application of the hinges are required for a successful clinical outcome [1, pp. 287–543], [2, Chapter 12]. Some small errors can cause major displacements of bone fragments, which is unacceptable clinically. Especially, treatment of rotational deformities are difficult because of bone translation during derotation maneuvers. Frequent revisions of the hinges are required in the course of treatment.

For an orthopaedic surgeon, without complex pre-oprative planning, application of a frame depending on clinical soft tissue and bone conditions, and to deal with residual displacements and deformity later would be simple. The main purpose of this study is to try to realize this concept.

Realization of the concept requires the effective application of spatial external fixators providing controlled motion capabilities with six degrees of freedom in 3-D space. This work aims to propose a mathematical model for an effective deployment of a Gough-Stewart Platform (G-S) Mechanism as a spatial external fixator.

2. Theory

It is by now a well-established fact that spatial fixators are used in medical practice, not only in the area of fracture treatment, but also towards the correction of bone deformities [3]. However, the quality of this service can only be improved by casting light on the biomechanical foundations of this practice. Thus, departing from such a point of view, we will show here how, by using a spatial fixator, the fractured bone fragments can be brought to their previously healthy positions before fracture or how movements of the ends resulting from cutting off the deformed bones can be controlled in a desirable way.

One of the very effective spatial fixators which might suitably be employed for the aforementioned orthopaedic purposes is the so-called G-S Platform Mechanism. First introduced as a universal tire-test machine by Gough [4] and later as a flight simulator by Stewart [5], a G-S platform has several modes of existence. An appropriate model of a G-S Platform Mechanism to be considered here consists of two platforms, one moving, the other fixed, whereby the fixed platform, called base, is connected to the moving platform by six bars through six double spherical joints. Such a robotic structure provides six degrees of freedom, three translational and three rotational in space. Thus, by changing the lengths of the bars, the relative position of the moving platform can be determined with respect to the base. The problem in which relative positions of the platforms can be estimated against given bar lengths is known as the direct (or forward) kinematics problem. The direct kinematics of G-S Platform Mechanisms have been worked out by many authors; see [6–11]. The inverse kinematic problem, in which bar lengths are computed for desired positions, has found interesting applications in different areas; see *e.g.*, [12, 13].

As a fixator, a G-S Platform Mechanism is applied in such a way that the base platform is connected rigidly to the proximal fragment, while the moving platform is located on the distal fragment. The circles circumscribing the base triangle ($A_1A_2A_3$) and the movable platform triangle ($B_1B_2B_3$) will be referred to as proximal and distal rings, respectively, both in concept and in the physical arrangement as shown in Figure 1(a). When the proximal and distal ring planes are parallel to each other, this is to be understood as the neutral configuration.

It is possible that the orthopaedist may join the fragments at the fracture site with the rings of the fixator in several different ways. In a first case, it is assumed that the bone fragments are fixed to the ring planes, so that the bone axes and plane normals are parallel. It may be thought, in a second case, that the bone axis is connected perpendicular to the ring plane in the proximal part of the fracture site, while the distal fragment is located arbitrarily on the relevant ring of the fixator. As a most general third case, it is probable that, both on the proximal and distal sides of the fixator, the fragment axes may have arbitrary configurations in relation to the ring planes. Furthermore, it is realistic to assume in all cases that the bone and ring centers are not coincident.

In dealing with the different cases, we will perform an inverse kinematic analysis on the G-S Platform model fixator. Input to that analysis will come from radiographic data as well as from clinical examination results. The analysis will provide the leg lengths (L_1–L_6) of the Stewart Platform Mechanism. As radiographic data, lateral and anteroposterior (AP) views projected along the x- and y-axes are needed, as shown in Figure 1(a). An axial view, when clinically performed, will yield further data for the analysis. The mentioned xyz co-ordinate system is located at the center of the proximal ring, G (Figure 1(a)), so that the xy-plane formed by the A_1, A_2, A_3 spherical joints is coincident with the base of the G-S Platform and the x-axis passes through the center of spherical joint A_1. The spherical joints B_1, B_2, B_3 seen in Figure 1(a) belong to the moving platform fixed to the distal fragment. The center of

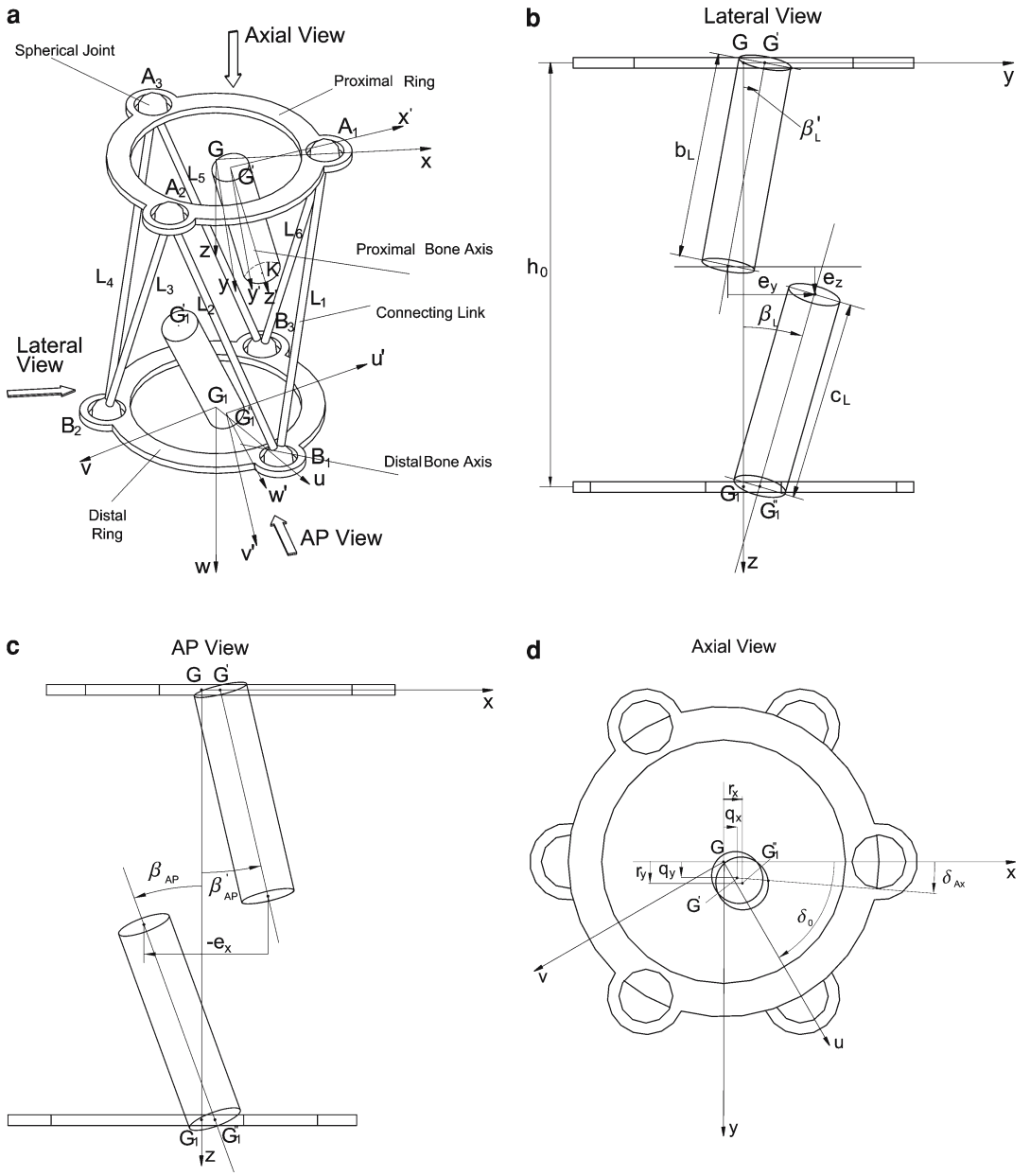

Figure 1. (a) General fixator assembly in neutral configuration (b) Measured parameters of fixator on lateral plane (c) Measured parameters of fixator on AP plane (d) Measured parameters of fixator on axial plane.

the distal ring G_1 will also be the origin of a movable *uvw* co-ordinate system attached to the moving platform, whereby the *uv*-plane is defined by the distal ring and the *u*-axis is defined by G_1B_1; see Figure 1(a).

Based on the above assumptions and notation, a detailed analyses of the three cases will be presented. See Appendix D for a list of symbols.

2.1. First case

We consider the situation as shown in Figure 2. Both bone fragments are perpendicular to the respective circles.

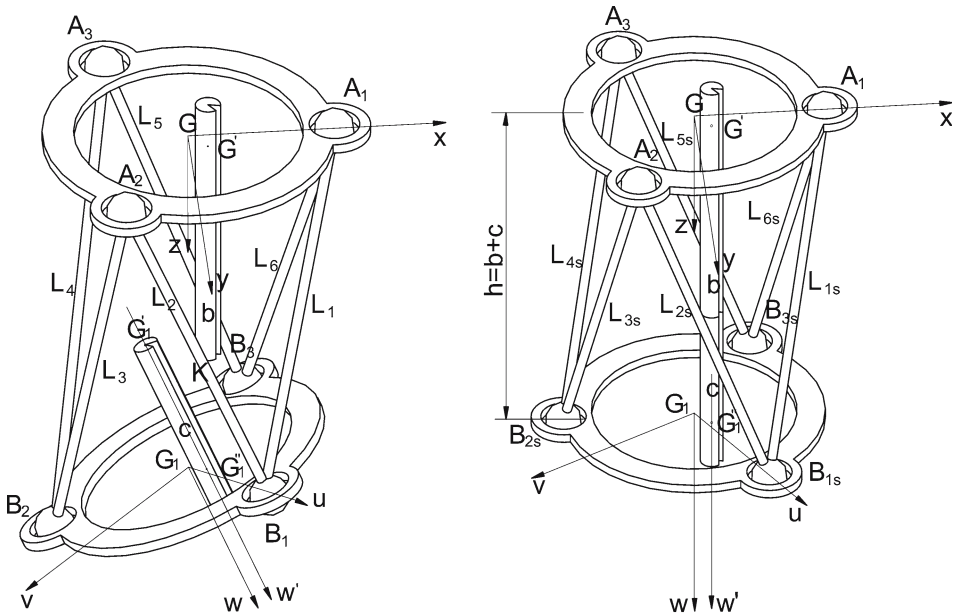

Figure 2. Case 1 of fixator assembly.

First, it is necessary to recognize the parameters which characterize the initial and final configurations of the Stewart Platform, one of them being the neutral configuration. The values of these parameters are to be taken from measurements on the lateral, AP, radiographs and on the axial clinical examinations; see Figure 1(b–d). Parameter h designates the distance between the proximal and distal ring planes along the z-direction, when the fixator is at its neutral configuration; see Figure 1(b). Parameters q_x, q_y signify the distances between the centers G of the proximal ring and G′ of the proximal fragment along the x,y-directions in the proximal ring plane, respectively; see Figure 1(d). Similarly, r_x, r_y, r_z are the corresponding distances, measured along the x,y,z axes, respectively, of the G_1'' distal bone axis from the distal ring center G_1 in the distal ring plane, in the fixed Gxyz-system; see Figure 1(d). Both axial clinical examination, as well as lateral and AP radiographs, are used to get data relevant to q_x, q_y, r_x, r_y, r_z for subsequent evaluation. The distances e_x, e_y, e_z are the quantities representing relative translations of the fragment bone ends along the x,y,z, axes, respectively, which are necessarily measured from lateral and AP radiographs, as shown in Figure 1(b), (c). The projected lengths b_L, c_L of the proximal and distal fragments on the lateral plane are shown in Figure 1(b). The angles β_L, β_{AP} are measured between the vertical z-axis and the projected axis of the distal fragment on the lateral (L) and on the AP planes, respectively, as shown in Figure 1(b), (c). Similar angle definitions apply for the parameters β'_L, β'_{AP}, this time for the proximal bone, as shown in Figure 1(b), (c). These angles can be easily determined from the AP and lateral radiographs. The projected relative angular displacement δ_{Ax} of the distal fragment with respect to the proximal fragment in the axial view is seen in Figure 1(d). Determination of δ_{Ax} makes it necessary to refer to clinical examination. Finally, parameter δ_0 designates the relative rotation of the distal ring with respect to the proximal ring, as shown in Figure 1(d). This angle can be pre-determined from the initial mounting configuration of the fixator as applied to the fracture site.

Given the above data and the accompanying assumptions, it will now be possible for us to express the unit vectors $\mathbf{e}_u$, $\mathbf{e}_v$, $\mathbf{e}_w$ of the moving co-ordinate system G_1uvw attached to the distal ring at G_1 according to the following calculations (see Appendix A).

$$\tan\beta_{Ax} = \frac{\tan\beta_{AP}}{\tan\beta_L}, \tag{1}$$

$$\tan\beta_{wz} = \frac{\tan\beta_{AP}}{\sin\beta_{Ax}}, \tag{2}$$

$$\tan\beta_{wy} = \frac{\sqrt{1+\tan^2\beta_{wz}\sin^2\beta_{Ax}}}{\tan\beta_{wz}\cos\beta_{Ax}}, \tag{3}$$

$$\tan\beta_{wx} = \frac{\sqrt{1+\tan^2\beta_{wz}\cos^2\beta_{Ax}}}{\tan\beta_{wz}\sin\beta_{Ax}}. \tag{4}$$

Computed β_{wx}, β_{wy}, β_{wz} parameters define the angles between the w-axis of the moving G_1uvw and the fixed x, y, z axes of the base $Gxyz$ co-ordinate systems, respectively. If the unit vectors of the $Gxyz$ system are designated by **i, j, k,** then unit vector $\mathbf{e}_w$ is defined as follows:

$$\mathbf{e}_w = \mathbf{i}\cos\beta_{wx} + \mathbf{j}\cos\beta_{wy} + \mathbf{k}\cos\beta_{wz}. \tag{5}$$

Next, assuming that G_1uvw-system is obtained by rotating the $Gxyz$ system about the x, y, z axes, by γ, η, α angles in that order (*i.e.*, first γ-rotation about x-axis, second η-rotation about y-axis and third α-rotation about z-axis), the rotation matrix, [14, Chapter 2], [15, Chapter 2], we can form rot$[\gamma, \eta, \alpha]$ out of unit vector components in the following way:

$$[A_{Gxyz}^{G_1uvw}] =^* \text{rot}[\gamma, \eta, \alpha] =^* [\mathbf{e}_u\ \mathbf{e}_v\ \mathbf{e}_w] =^* \begin{bmatrix} e_{ux} & e_{vx} & e_{wx} \\ e_{uy} & e_{vy} & e_{wy} \\ e_{uz} & e_{vz} & e_{wz} \end{bmatrix}. \tag{6}$$

Here the entries $e_{ux}, e_{uy}, e_{uz}, e_{vx}, e_{vy}, e_{vz}, e_{wx}, e_{wy}, e_{wz}$ of the matrix are the components of the unit vectors $\mathbf{e}_u$, $\mathbf{e}_v$, $\mathbf{e}_w$ along the fixed *x, y, z* axes. The matrix $A_{Gxyz}^{G_1uvw}$ can also be viewed as a transformation matrix mapping distal-ring-attached points into the base-attached reference frame, except for translation. If the rotation matrix is rewritten in terms of the angles γ, η, α, then [14, Chapter 2]:

$$[A_{Gxyz}^{G_1uvw}] = \begin{bmatrix} \cos\alpha\cos\eta & \cos\alpha\sin\eta\sin\gamma - \sin\alpha\cos\gamma & \cos\alpha\sin\eta\cos\gamma + \sin\alpha\sin\gamma \\ \sin\alpha\cos\eta & \sin\alpha\sin\eta\sin\gamma + \cos\alpha\cos\gamma & \sin\alpha\sin\eta\cos\gamma - \cos\alpha\sin\gamma \\ -\sin\eta & \cos\eta\sin\gamma & \cos\eta\cos\gamma \end{bmatrix}. \tag{7}$$

Knowing the components of $\mathbf{e}_w$ along the normal of the distal ring plane from (5), we can make use of the last column of the transformation matrix in (7) in the calculation of the unit vectors $\mathbf{e}_u$ and $\mathbf{e}_v$. To this end, inserting $(\delta_0 - \delta_{Ax})$ as α in (7) and solving the equations resulting from comparison of (7) with (6) for the unknown angles we obtain the following:

$$\tan\eta = \frac{e_{wx}\cos(\delta_0 - \delta_{Ax}) + e_{wy}\sin(\delta_0 - \delta_{Ax})}{e_{wz}}, \tag{8}$$

$$\cos\gamma = \frac{e_{wz}}{\cos\eta}. \tag{9}$$

The relationships (8), (9) now define the unit vectors $\mathbf{e}_u$, $\mathbf{e}_v$, $\mathbf{e}_w$.

From the given set (b_L, c_L), one can calculate the fragment lengths on the proximal (b) and distal sides (c) of the fracture point. Since fragments are assumed to be perpendicular to their relevant planes of attachment in the first case, Figure 2(a), on the base part it is apparent that $b_L = b$, whereas on the moving part, c will be estimated by the following:

$$c = \frac{c_L}{\sqrt{\cos^2 \beta_{wz} + \cos^2 \beta_{Ax} \sin^2 \beta_{wz}}}. \tag{10}$$

With reference to Figure 2(a), G_1' is the fracture point on the distal fragment to be unified with its counterpart K on the proximal fragment. Accordingly, the following vector relationships can be written down in the fixed Gxyz-system:

$$\mathbf{GG}_1 = \mathbf{GK} + \mathbf{KG}_1' + \mathbf{G}_1'\mathbf{G}_1'' - \mathbf{G}_1\mathbf{G}_1'' \tag{11}$$

with

$$\mathbf{GK} = q_x\mathbf{i} + q_y\mathbf{j} + b\mathbf{k}, \tag{12}$$
$$\mathbf{KG}_1' = e_x\mathbf{i} + e_y\mathbf{j} + e_z\mathbf{k}, \tag{13}$$
$$\mathbf{G}_1\mathbf{G}_1'' = r_x\mathbf{i} + r_y\mathbf{j} + r_z\mathbf{k}, \tag{14}$$
$$\mathbf{G}_1'\mathbf{G}_1'' = c\mathbf{e}_\mathbf{w} = c(e_{wx}\mathbf{i} + e_{wy}\mathbf{j} + e_{wz}\mathbf{k}). \tag{15}$$

Furthermore:

$$\mathbf{GB}_1 = \mathbf{GG}_1 + \mathbf{G}_1\mathbf{B}_1, \tag{16}$$
$$\mathbf{GB}_2 = \mathbf{GG}_1 + \mathbf{G}_1\mathbf{B}_2, \tag{17}$$
$$\mathbf{GB}_3 = \mathbf{GG}_1 + \mathbf{G}_1\mathbf{B}_3. \tag{18}$$

Now, in order to calculate $\mathbf{G}_1\mathbf{B}_1$, $\mathbf{G}_1\mathbf{B}_2$, $\mathbf{G}_1\mathbf{B}_3$, one can imagine a triangle $B_1B_2B_3$ with sides b_1=B_2B_3, b_2=B_3B_1, b_3=B_1B_2 and describe the vectors in the moving G$_1uvw$-system:

$$\mathbf{G}_1\mathbf{B}_1 = R_1\mathbf{e}_u, \tag{19}$$
$$\mathbf{G}_1\mathbf{B}_2 = -R_1 \cos 2\delta_1 \mathbf{e}_u + R_1 \sin 2\delta_1 \mathbf{e}_v, \tag{20}$$
$$\mathbf{G}_1\mathbf{B}_3 = -R_1 \cos 2\delta_3 \mathbf{e}_u - R_1 \sin 2\delta_3 \mathbf{e}_v, \tag{21}$$

where: (see Appendix B)

$$\delta_1 = \frac{\varphi_1 + \varphi_2 - \varphi_3}{2}; \quad \delta_3 = \frac{\varphi_3 + \varphi_1 - \varphi_2}{2}; \quad R_1 = \frac{b_2}{2\cos\,\delta_3}, \tag{22}$$

$$\varphi_1 = \cos^{-1}\left(\frac{b_2^2 + b_3^2 - b_1^2}{2b_2b_3}\right); \quad \varphi_2 = \cos^{-1}\left(\frac{b_3^2 + b_1^2 - b_2^2}{2b_3b_1}\right); \quad \varphi_3 = \cos^{-1}\left(\frac{b_1^2 + b_2^2 - b_3^2}{2b_1b_2}\right). \tag{23}$$

Since $\mathbf{e}_u$, $\mathbf{e}_v$ have already been defined in terms of the Gxyz-system unit vectors by either (6) or (7), the vectors under consideration are clearly well-known now in the fixed Gxyz-system.

With a similar reasoning in the proximal ring plane, $A_1A_2A_3$ can be imagined as a triangle with sides a_1=A_2A_3, a_2=A_3A_1, a_3=A_1A_2; see Figure 2(a). Then, the vectors $\mathbf{GA}_1$, $\mathbf{GA}_2$, $\mathbf{GA}_3$ in the fixed Gxyz-system will identify the co-ordinates of the points A_1, A_2, A_3, respectively.

$$\mathbf{GA}_1 = R\mathbf{i}, \tag{24}$$

$$\mathbf{GA}_2 = -R\cos 2\beta_1\mathbf{i} + R\sin 2\beta_1\mathbf{j}, \tag{25}$$

$$\mathbf{GA}_3 = -R\cos 2\beta_3\mathbf{i} - R\sin 2\beta_3\mathbf{j}, \tag{26}$$

where:

$$\beta_1 = \frac{\phi_1+\phi_2-\phi_3}{2}; \quad \beta_3 = \frac{\phi_3+\phi_1-\phi_2}{2}; \quad R = \frac{a_2}{2\cos\,\beta_3}, \tag{27}$$

$$\phi_1 = \cos^{-1}\left(\frac{a_2^2+a_3^2-a_1^2}{2a_2a_3}\right); \quad \phi_2 = \cos^{-1}\left(\frac{a_3^2+a_1^2-a_2^2}{2a_3a_1}\right); \quad \phi_3 = \cos^{-1}\left(\frac{a_1^2+a_2^2-a_3^2}{2a_1a_2}\right). \tag{28}$$

When the platform is in its first configuration, Figure 2(a), the bar lengths (L_1–L_6) can be evaluated by taking into account distance formulae between the relevant points specified in the same system:

$$L_{2i-1} = |\mathbf{GA}_i - \mathbf{GB}_i|; \quad L_{2i} = \left|\mathbf{GA}_j - \mathbf{GB}_i\right|, \quad i = 1, 2, 3; \quad j = -2 + 5{\cdot}5i - 1{\cdot}5i^2 \tag{29}$$

For the final configuration of the platform, Figure 2(b), the link lengths $L_{1s}, L_{2s}, L_{3s}, L_{4s}, L_{5s}$, L_{6s} are computed in the same way by the formula (29), except that, $\mathbf{GA}_1$, $\mathbf{GA}_2$, $\mathbf{GA}_3$ being same, the vectors $\mathbf{GB}_1$, $\mathbf{GB}_2$, $\mathbf{GB}_3$ are replaced by $\mathbf{GB}_{1s}$, $\mathbf{GB}_{2s}$, $\mathbf{GB}_{3s}$ as given below:

$$\mathbf{GB}_{1s} = (R_1\cos\delta_0 + q_x - r_x)\mathbf{i} + (R_1\sin\delta_0 + q_y - r_y)\mathbf{j} + (b+c)\mathbf{k} \tag{30}$$

$$\mathbf{GB}_{2s} = (-R_1\cos(2\delta_1 - \delta_0) + q_x - r_x)\mathbf{i} + (R_1\sin(2\delta_1 - \delta_0) + q_y - r_y)\mathbf{j} + (b+c)\mathbf{k} \tag{31}$$

$$\mathbf{GB}_{3s} = (-R_1\cos(2\delta_3 + \delta_0) + q_x - r_x)\mathbf{i} + (-R_1\sin(2\delta_3 + \delta_0) + q_y - r_y)\mathbf{j} + (b+c)\mathbf{k} \tag{32}$$

2.2. Second case

The second case may result for several reasons. One of these might be that, after imposing the requirements of the first case and after fracture fixation, radiographs and clinical investigations might point to a residual deformity at the neutral configuration. In that case, all the characteristic data pertaining to the parameters described in the first case, as shown in Figure 1, should be determined again and re-evaluated in such a way that, with proper bar lengths, the bone is finally brought to its anatomically correct position, as shown in Figure 3(b). Here it is to be understood that proximal parts retain their normal positions, while the relative positions of the distal parts have taken on an arbitrary appearance, as shown in Figure 3(a).

In addition to the co-ordinate systems Gxyz and G$_1uvw$ defined earlier, (*cf*. Figure 1(a)), one more reference frame $G_1''u'v'w'$ with origin at the point of intersection, G_1'', of distal fragment axis (w') with the distal ring plane $B_1B_2B_3$ is needed to formulate the process. Unit vectors of each reference system will be obtained through the transformation matrices both at the initial and final configurations of the fixator assembly, as shown in Figure 3. Since the Guvw system is obtained by rotating the Gxyz reference system through an angle δ_0 about the z-axis, the transformation matrix $[A_{Gxyz}^{G_1uvw}]_1$ and hence the unit vectors $[\mathbf{e}_u\ \mathbf{e}_v\ \mathbf{e}_w]_1$ at the initial configuration "1", are determined by setting $\gamma = 0, \eta = 0$ and $\alpha = \delta_0$ in (7). Following a very similar procedure as in the first case by taking into account the recorded data as well as Equations (1–9) except that α is set equal to δ_{Ax} in (8) and (9), we may compute the rotation matrix $[A_{Gxyz}^{G_1''u'v'w'}]_1$ which expresses the unit vectors $[\mathbf{e}_{u'}\,\mathbf{e}_{v'}\,\mathbf{e}_{w'}]_1$ of the $G_1''u'v'w'$-system with respect to the fixed Gxyz-system in configuration "1". Then, because of the orthonormal properties of rotation matrices, the transformation of the G$_1uvw$-system relative

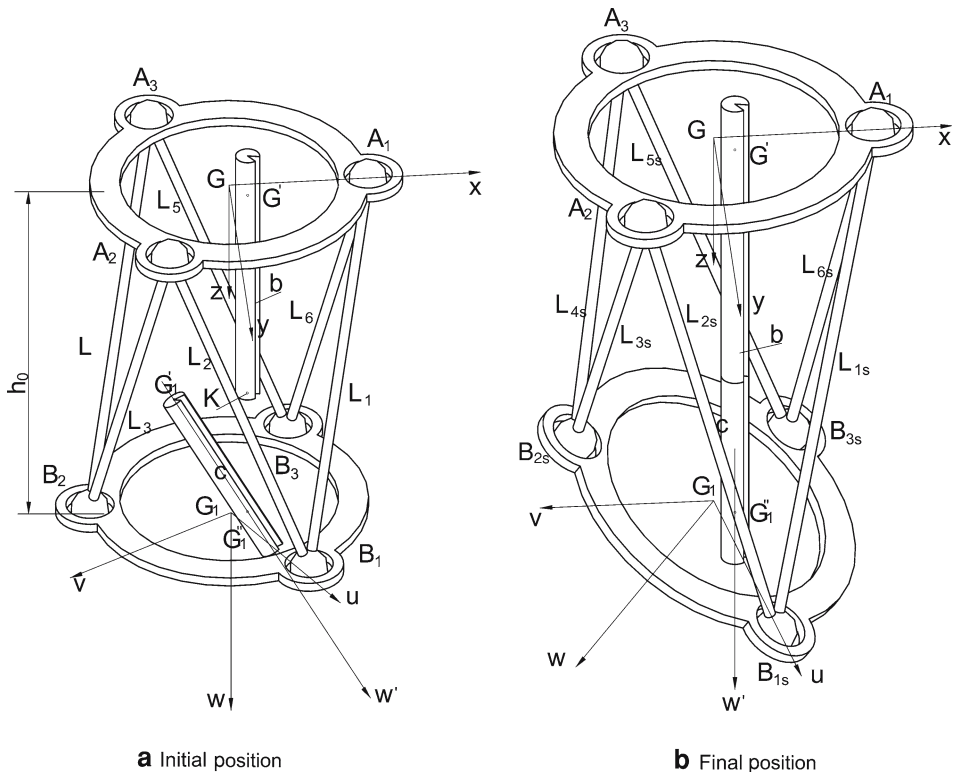

a Initial position **b** Final position

Figure 3. Case 2 of fixator assembly.

to the $G_1''u'v'w'$-system, represented by the matrix $[A^{G_1uvw}_{G_1''u'v'w'}]_1$, is estimated from the following matrix product:

$$[A^{G_1uvw}_{G_1''u'v'w'}]_1 = [A^{G_1''u'v'w'}_{Gxyz}]_1^{\mathrm{T}}\,[A^{G_1uvw}_{Gxyz}]_1, \tag{33}$$

where superscript T denotes the transpose.

In configuration "2" of the fixator assembly, Figure 3(b), similar to (33), the following can be written for the rotation matrices:

$$[A^{G_1uvw}_{Gxyz}]_2 = [A^{G_1''u'v'w'}_{Gxyz}]_2\,[A^{G_1uvw}_{G_1''u'v'w'}]_2. \tag{34}$$

However, since the axes of the $G_1''u'v'w'$ and those of the fixed Gxyz systems become parallel, we have

$$[A^{G_1''u'v'w'}_{Gxyz}]_2 =^{*} [\mathbf{e}_{u'}\,\mathbf{e}_{v'}\,\mathbf{e}_{w'}]_2 = \begin{bmatrix} 1 & 0 & 0 \\ 0 & 1 & 0 \\ 0 & 0 & 1 \end{bmatrix}. \tag{35}$$

It is also clear that, since both the G$_1uvw$ and the $G_1''u'v'w'$ systems are attached to the same distal platform, a relative transformation amongst them remains invariant under any change of configuration. Thus:

$$[A^{G_1uvw}_{G_1''u'v'w'}]_2 = [A^{G_1uvw}_{G_1''u'v'w'}]_1. \tag{36}$$

From (34), in the light of (35) and (36), it follows:

$$[A^{G_1uvw}_{Gxyz}]_2 =^{*} [\mathbf{e}_u\,\mathbf{e}_v\,\mathbf{e}_w]_2 = [A^{G_1uvw}_{G_1''u'v'w'}]_1. \tag{37}$$

Based on the above discussion, first the link lengths (L_1–L_6) are computed to correspond to the initial configuration, Figure 3(a), by evaluating $\mathbf{GB}_1$, $\mathbf{GB}_2$, $\mathbf{GB}_3$ as given below under (38–40) and then substituting them in (29):

$$\mathbf{GB}_1 = R_1 \cos\delta_0 \mathbf{i} + R_1 \sin\delta_0 \mathbf{j} + h_0 \mathbf{k}, \tag{38}$$

$$\mathbf{GB}_2 = -R_1 \cos(2\delta_1 - \delta_0)\mathbf{i} + R_1 \sin(2\delta_1 - \delta_0)\mathbf{j} + h_0 \mathbf{k}, \tag{39}$$

$$\mathbf{GB}_3 = -R_1 \cos(2\delta_3 + \delta_0)\mathbf{i} + -R_1 \sin(2\delta_3 + \delta_0)\mathbf{j} + h_0 \mathbf{k}, \tag{40}$$

where h_0 is the initial height between the base and the moving platforms along the z-axis and R_1 is the distal ring radius associated with δ_1, δ_3 in (22) and (23). As for the link lengths (L_{1s}–L_{6s}) in the final configuration, these are calculated by the following vector relationships, with reference to Figure 3(b):

$$\mathbf{GG}_1 = \mathbf{GG}' + \mathbf{G}'\mathbf{G}_1'' - \mathbf{G}_1\mathbf{G}_1'', \tag{41}$$

$$\mathbf{GG}' = q_x \mathbf{i} + q_y \mathbf{j}, \tag{42}$$

$$\mathbf{G}'\mathbf{G}_1'' = (b + c)\mathbf{k}, \tag{43}$$

$$\mathbf{G_1G_1''} = (r_u e_{u'x} + r_v e_{v'x})\mathbf{i} + (r_u e_{u'y} + r_v e_{v'y})\mathbf{j} + (r_u e_{u'z} + r_v e_{v'z})\mathbf{k}. \tag{44}$$

Here b, c are the proximal and distal fragment lengths, respectively; $e_{u'x}$, $e_{u'y}$, $e_{u'z}$, $e_{v'x}$, $e_{v'y}$, $e_{v'z}$, $e_{w'x}$, $e_{w'y}$, $e_{w'z}$ are the entries of the matrix $[A_{Gxyz}^{G_1''u'v'w'}]_1$ and r_u,r_v are the components estimated from (r_x, r_y) radiographic data as follows:

$$r_u = r_x \cos\delta_0 + r_y \sin\delta_0, \tag{45}$$

$$r_v = -r_x \sin\delta_0 + r_y \cos\delta_0. \tag{46}$$

Completion of evaluations is realized by considering Equations (16–29) with the help of (37).

2.3. Third case

During the attachment phase of the platforms to the fragments at the fracture site, the orthopaedist may fail to comply with the assumptions of the previous two cases or the correction of a residual deformity may be desired. As a result, the fragments may have been attached to the rings on both the proximal and the distal sides of the fracture in an oblique position, bringing the inverse kinematic problem into the subject matter of the third case.

In the third case, a new co-ordinate system $G'x'y'z'$ (*c.f.* Figure 1(a)) is required at point G′, where the proximal fragment axis meets with the proximal ring plane, in order to describe the oblique position of the proximal bone. The system $G'x'y'z'$ is obtained by rotating the Gxyz-system about the fixed x, y, z-axes through the angles γ', η' and $\alpha' = 0$, respectively (*i.e.*, first a γ'-rotation about the x-axis, then a η'-rotation about the y-axis). Thus, the description of the G′$x'y'z'$-system with respect to the reference frame Gxyz is to be made as follows:

$$[A_{Gxyz}^{Gx'y'z'}] =^* [\mathbf{e}_{x'}\ \mathbf{e}_{y'}\ \mathbf{e}_{z'}] = \begin{bmatrix} \cos\eta' & \sin\eta'\sin\gamma' & \sin\eta'\cos\gamma' \\ 0 & \cos\gamma' & -\sin\gamma' \\ -\sin\eta' & \cos\eta'\sin\gamma' & \cos\eta'\cos\gamma' \end{bmatrix}. \tag{47}$$

Now, by referring to the radiographic data collected from the lateral and AP views, (*i.e.*, β_L', $\beta_{\mathbf{AP}}'$) one can define the orientation of the z'-axis as follows:

$$\mathbf{e}_{z'} = \mathbf{i}\cos\beta_{z'x} + \mathbf{j}\cos\beta_{z'y} + \mathbf{k}\cos\beta_{z'z}, \tag{48}$$

where $\beta_{z'x}$, $\beta_{z'y}$, $\beta_{z'z}$ are determined according to the following relationships:

$$\tan \beta'_{Ax} = \frac{\tan \beta'_{AP}}{\tan \beta'_{L}}, \tag{49}$$

$$\tan \beta_{z'z} = \frac{\tan \beta'_{AP}}{\sin \beta'_{Ax}}, \tag{50}$$

$$\tan \beta_{z'y} = \frac{\sqrt{1 + \tan^2 \beta_{z'z} \sin^2 \beta'_{Ax}}}{\tan \beta_{z'z} \cos \beta'_{Ax}}, \tag{51}$$

$$\tan \beta_{z'x} = \frac{\sqrt{1 + \tan^2 \beta_{z'z} \cos^2 \beta'_{Ax}}}{\tan \beta_{z'z} \sin \beta'_{Ax}}. \tag{52}$$

By comparison of (48) with (47), the following is deduced:

$$\tan \eta' = \frac{\cos \beta_{z'x}}{\cos \beta_{z'z}}, \tag{53}$$

$$\cos \gamma' = \frac{\cos \beta_{z'z}}{\cos \eta'}. \tag{54}$$

Thus the rotation matrix $[A_{Gxyz}^{G'x'y'z'}]$ in (47) is now well-defined.

The third case is also characterized by the initial and final configurations of the fixator assembly, as shown in Figure 4(a), (b). Since the description of the first configuration in the third case is not affected by the oblique position of the proximal part, the neutral position will be handled in the same way as in the second case, as shown in Figure 4(a) and in Figure 3(a). The distal part being the same in both cases, equations and conditions like (33), (34), (36), (37) will hold true for the third case too. Different, however, from the second case is the fact that the axes of the $G'x'y'z'$ and $G''_1u'v'w'$ systems are to be parallel in the final configuration of the third case, Figure 4(b), which is expressed by the following:

$$[A_{Gxyz}^{G''_1u'v'w'}]_2 = [\mathbf{e}_{u'}\ \mathbf{e}_{v'}\ \mathbf{e}_{w'}]_2 = [\mathbf{e}_{x'}\ \mathbf{e}_{y'}\ \mathbf{e}_{z'}]. \tag{55}$$

Thus, in order to get $[A_{Gxyz}^{G_1uvw}]_2$, specific for the third case, Equation (55) is substituted in (34) together with (33) and all other calculations are the same as in the second case. After transforming the co-ordinates of the points B_1, B_2, B_3 into the fixed reference-frame co-ordinates in the initial "1" and final "2" configurations, Equation (29) can be employed to obtain the leg lengths.

3. Motion of the fixator

Important in all the previous cases were only the two configurations of the fixator assembly, one at the time of fixation, the other which is the anatomically desirable one. Nevertheless, how the transition between initial and final configurations will materialize is a problem to be resolved. Thus, this problem makes it necessary to look at the motion of the fixator.

All the previous cases can be regarded within the context of the inverse kinematic problem. However, the motion of the fixator is a direct kinematic problem. When the link lengths in the G-S Platform fixator are assigned new values, the position of the distal fragment fixed to the moving platform will change relative to the proximal fragment attached to the base. In this way, the ends of the fragments will move closer to each other, finally ending in the union

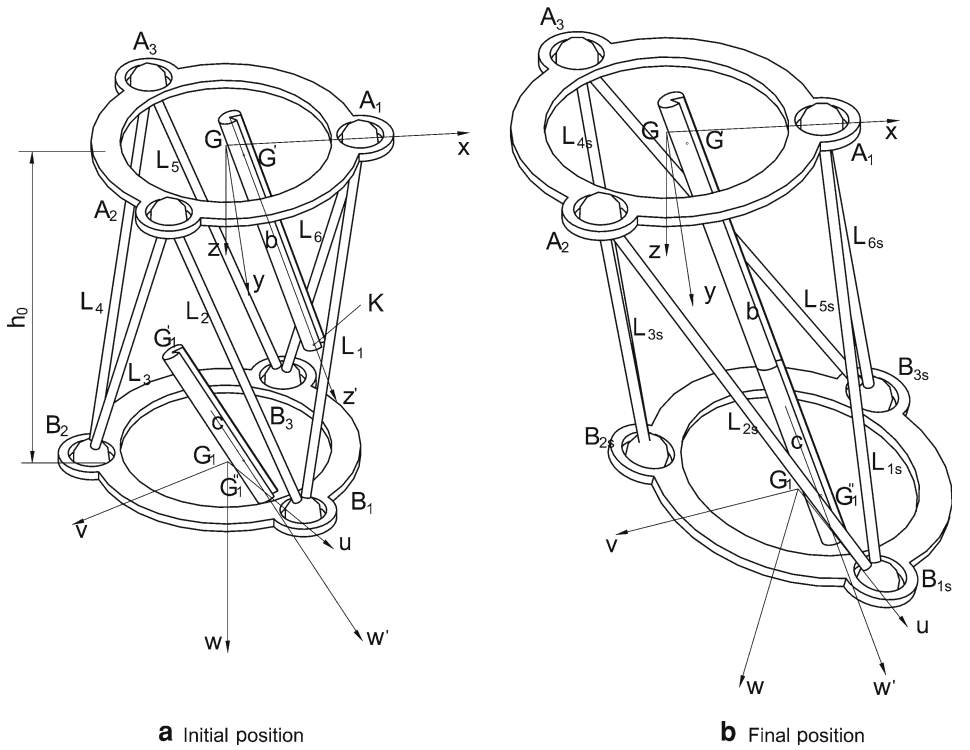

Figure 4. Case 3 of fixator assembly.

position. Here, in this process, the trajectory of the distal fragment end may be of interest to the orthopaedist to remain within the physically allowable limits from a medical point of view. Moreover, for reasons of medical-treatment strategies or planning, it may be necessary to know the amounts of linear and angular displacements of fragments relative to each other. There is a need to examine the motion of the G-S Platform Mechanism as a fixator.

The analysis of the motion will be carried out in a systematic manner to be useful in medical planning. For this purpose, the following steps will be executed:

(i) Differences in each link length corresponding to the initial and final configurations of the Stewart Platform, as determined previously, are calculated, *i.e.*,

$$\Delta L_j = L_{js} - L_j, \quad j = 1 \ldots 6. \tag{56}$$

(ii) In accordance with the requirements of a medical-treatment strategy, the number of steps in which the link lengths are modified is selected as a positive integer (n), with which length increments or decrements (ΔS_i) are prescribed:

$$\Delta S_j = \frac{\Delta L_j}{n}. \tag{57}$$

(iii) Each length in the fixator mechanism is adjusted to its new value as follows:

$$L_{ji} = L_j + i\,\Delta S_j, \quad j = 1 \ldots 6, \quad i = 0, \ldots, n. \tag{58}$$

According to the direct kinematic analysis, [6, 7, 11], for a given set of L_{ji} in each step, there are sixteen different positions of the points $B_{1i}, B_{2i}, B_{3i}, i = 0, \ldots, n$, but only one position satisfies the initial ($L_j = L_{j0}, i = 0$) and final ($L_{js} = L_{jn}, i = n$) values of the link lengths as determined

in the previous three cases. After deciding on the correct positions of the points (B_{1i}, B_{2i}, B_{3i}) in each step, which characterize the motion of the moving platform, a decoupling process is started to decompose the resultant motion into the translation along the three axes of the Gxyz-fixed reference frame and rotation about the fixed x, y, z-axes. With a knowledge of B_{1i}, B_{2i}, B_{3i} co-ordinates, Equations (16–18) are solved with the help of (19–23), to get $\mathbf{e}_u$, $\mathbf{e}_v$ and $\mathbf{e}_w$ as the cross-product of the unit vectors $\mathbf{e}_u$, $\mathbf{e}_v$, of the G$_1uvw$-system, which then leads to the co-ordinates of G$_1$, namely $g_{1xi}, g_{1yi}, g_{1zi}$, as follows: (See Appendix C).

$$g_{1xi} = \frac{1}{4\cos\delta_3\cos\delta_1\sin(\delta_3+\delta_1)}\left[B_{1xi}\sin(2\delta_3+2\delta_1) + B_{2xi}\sin 2\delta_3 + B_{3xi}\sin 2\delta_1\right], \tag{59}$$

$$g_{1yi} = \frac{1}{4\cos\delta_3\cos\delta_1\sin(\delta_3+\delta_1)}\left[B_{1yi}\sin(2\delta_3+2\delta_1) + B_{2yi}\sin 2\delta_3 + B_{3yi}\sin 2\delta_1\right], \tag{60}$$

$$g_{1zi} = \frac{1}{4\cos\delta_3\cos\delta_1\sin(\delta_3+\delta_1)}\left[B_{1zi}\sin(2\delta_3+2\delta_1) + B_{2zi}\sin 2\delta_3 + B_{3zi}\sin 2\delta_1\right], \tag{61}$$

$$\mathbf{e}_{ui} = \frac{(B_{1xi}-g_{1xi})}{R_1}\mathbf{i} + \frac{(B_{1yi}-g_{1yi})}{R_1}\mathbf{j} + \frac{(B_{1zi}-g_{1zi})}{R_1}\mathbf{k}, \tag{62}$$

$$\mathbf{e}_{vi} = \frac{1}{\sin(2\delta_3+2\delta_1)R_1}\begin{bmatrix}[(B_{2xi}-g_{1xi})\cos 2\delta_3 - (B_{3xi}-g_{1xi})\sin 2\delta_1]\mathbf{i} + \\ \left[(B_{2yi}-g_{1yi})\cos 2\delta_3 - (B_{3yi}-g_{1yi})\sin 2\delta_1\right]\mathbf{j} + \\ [(B_{2zi}-g_{1zi})\cos 2\delta_3 - (B_{3zi}-g_{1zi})\sin 2\delta_1]\mathbf{k} + \end{bmatrix}, \tag{63}$$

$$\mathbf{e}_{wi} = (e_{uyi}e_{vzi} - e_{uzi}e_{vyi})\mathbf{i} + (e_{uzi}e_{vxi} - e_{uxi}e_{vzi})\mathbf{j} + (e_{uxi}e_{vyi} - e_{uyi}e_{vxi})\mathbf{k}, \tag{64}$$

where $(B_{1xi}, B_{1yi}, B_{1zi})$, $(B_{2xi}, B_{2yi}, B_{2zi})$, $(B_{3xi}, B_{3yi}, B_{3zi})$ are the coordinates of B_1, B_2, B_3, respectively, in the Gxyz-system at step i. By means of (62–64), the rotation matrix $[A^{G_1uvw}_{G''_1xyz}]_i$ at i-th step is constructed:

$$[A^{G_1uvw}_{Gxyz}]_i = [\mathbf{e}_{ui}\ \mathbf{e}_{vi}\ \mathbf{e}_{wi}] = \begin{bmatrix} e_{ux} & e_{vx} & e_{wx} \\ e_{uy} & e_{vy} & e_{wy} \\ e_{uz} & e_{vz} & e_{wz} \end{bmatrix}. \tag{65}$$

Thus, the rotation angles (γ, η, α) about the x, y, z-axes are extracted in that order from the matrix above as follows [14, Chapter 2]:

$$\gamma_i = \tan^{-1}(e_{vzi}/e_{wzi}), \tag{66}$$

$$\eta_i = \tan^{-1}\left(-e_{uzi}/\sqrt{e^2_{uxi}+e^2_{uyi}}\right), \tag{67}$$

$$\alpha_i = \tan^{-1}(e_{uyi}/e_{uxi}). \tag{68}$$

With (59–61) and (66–68), the three translations $(g_{1xi}, g_{1yi}, g_{1zi})$ and the three orderly rotations $(\gamma_i, \eta_i, \alpha_i)$ are now well-defined.

In order to describe the trajectory to be traced by the distal fragment end G$'_1$ during the treatment process in the fixed Gxyz-system, the following vector equation is written down for each step i:

$$\mathbf{GG}'_{1i} = \mathbf{GG}_{1i} + \mathbf{G}_{1i}\mathbf{G}''_{1i} - \mathbf{G}'_{1i}\mathbf{G}''_{1i}. \tag{69}$$

For the first case, Figure 2, vectors of interest are computed as follows:

$$\mathbf{G}_{1i}\mathbf{G}''_{1i} = r_u \mathbf{e}_{ui} + r_v \mathbf{e}_{vi}, \tag{70}$$

$$\mathbf{GG}_{1i} = g_{1xi}\mathbf{i} + g_{1yi}\mathbf{j} + g_{1zi}\mathbf{k}, \tag{71}$$

$$\mathbf{G}'_{1i}\mathbf{G}''_{1i} = c\mathbf{e}_{wi}, \tag{72}$$

where r_u, r_v are the same as in (45) and (46).

For the second and third cases, however, Equations (70) and (71) remaining the same, the vector $\mathbf{G}'_{1i}\mathbf{G}''_{1i}$ is determined in the following way:

$$\mathbf{G}'_{1i}\mathbf{G}''_{1i} = c\mathbf{e}_{w'i}, \tag{73}$$

where $\mathbf{e}_{w'}$ is the last column of the transformation matrix $[A^{G''_1 u'v'w'}_{Gxyz}]_i$ is expressed as follows:

$$[A^{G''_1 u'v'w'}_{Gxyz}]_i = [A^{G_1 uvw}_{Gxyz}]_i \, [A^{G_1 uvw}_{G''_1 u'v'w'}]^T. \tag{74}$$

In (74), $[A^{G_1 uvw}_{G''_1 u'v'w'}]$ is the same as defined in (33).

A rearrangement of (11) for the fracture opening ($\mathbf{KG}'_1$) may also be used in order to get an idea of how the ends of the fragments are positioned with respect to each other, at each intermediate step i of the treatment-planning process.

4. Numerical examples and discussion

Here, the three cases analyzed earlier will be illustrated in order to verify numerically the theory presented. Trajectories for each case will be obtained for three different examples. Common data for all the three examples come from only the upper $A_1A_2A_3$ ($a_1 = 10$, $a_2 = 10$, $a_3 = 10$), and lower $B_1B_2B_3$ ($b_1 = 10$, $b_2 = 10$, $b_3 = 10$) triangles. Wherever needed, direct kinematic analysis results have been taken from [6].

4.1. Example 1

In addition to the physical dimensions of the fixator, lateral, AP radiographic data, as well as the clinical investigation results are given. Required are the link lengths in the initial and final configurations of case 1, Section 2.1, motion results and fracture opening.

The Lateral data are specified as follows:

$e_y = -1{\cdot}70$ cm; $e_z = 0{\cdot}21$ cm; $c_L = 7{\cdot}58$ cm; $b = 12$ cm; $\beta_L = 12{\cdot}48^\circ$.
The AP data: $e_x = -2{\cdot}59$ cm; $\beta_{AP} = 19{\cdot}01^\circ$.
The Axial data: $q_x = 0{\cdot}50$ cm; $q_y = 0{\cdot}60$ cm; $r_x = 0{\cdot}70$ cm; $r_y = 0{\cdot}80$ cm; $\delta_0 = 60^\circ$; $\delta_{Ax} = -3{\cdot}87^\circ$.

First, for the data given above inverse kinematics involving the calculation procedure presented in Section 2.1 corresponding to case 1 is applied and leads to the following results:

$c = 8{\cdot}00$ cm; $L_1 = 18{\cdot}86$; $L_2 = 18{\cdot}82$; $L_3 = 22{\cdot}50$; $L_4 = 22{\cdot}58$; $L_5 = 20{\cdot}89$; $L_6 = 21{\cdot}09$.
$L_{1s} = 20{\cdot}80$; $L_{2s} = 20{\cdot}76$; $L_{3s} = 20{\cdot}89$; $L_{4s} = 20{\cdot}80$; $L_{5s} = 20{\cdot}76$; $L_{6s} = 20{\cdot}89$.

Secondly, the direct kinematics is carried out with the resulting lengths in the initial (L_1–L_6) and in the final (L_{1s}–L_{6s}) configurations of the G-S platform, leading to the coordinates of the distal ring joints B_1, B_2, B_3 as displayed in Table 1. It is clearly observed in Table 1 that if the orthopaedist uses the leg lengths estimated at the end of the inverse kinematics procedure (*i.e.*, Section 2.1), he (or she) is supposed to get the intended final neutral configuration, whereby the distal ring plane is parallel to the proximal one.

A ten-step treatment strategy is considered here to move from the initial configuration to the final one. The leg lengths are computed at each step in accordance with Equations (56–58) and are collected in Table 2. The significance of the values in Table 2 is that it produces for the orthopaedist the necessary values of the leg lengths to be applied to the G-S platform fixator at each step of the treatment strategy.

For the calculated leg lengths at each step, direct kinematics together with the theory presented in Section 3 is implemented yielding the B_1, B_2, B_3 co-ordinates and the fracture opening ($\mathbf{KG}_1'$) as shown in Table 3. While there is a totally (linear and angular) misaligned position of the bone fragments at the initial configuration (*i.e.*, step 0), all the misalignments have been removed in the final configuration (*i.e.*, step 10).

4.2. Example 2

The dimensions of the fixator, the lateral and AP views, as well as the clinical data, are input to the second case; see Figure 3. The output are the link lengths and motion results.

The specified lateral data are as follows: $e_y = 1{\cdot}03$ cm; $e_z = 1{\cdot}00$ cm; $c_L = 7.05$ cm; $b = 12$ cm; $\beta_L = -6{\cdot}75^0$.
The AP data: $e_x = -3{\cdot}58$ cm; $\beta_{AP} = 28{\cdot}34^\circ$.
The Axial data: $q_x = 0{\cdot}50$ cm; $q_y = 0{\cdot}60$ cm; $r_x = 0{\cdot}70$ cm; $r_y = 0{\cdot}80$ cm; $\delta_0 = 60^\circ$; $\delta_{Ax} = 20{\cdot}00^\circ$.

Table 1. Co-ordinates of points B_1, B_2, B_3 in Example 1.

		Co-ordinates		
Position	Points	x-Component	y-Component	z-Component
Initial	B_1	2·51	4·50	18·03
	B_2	−5·67	0·17	21·80
	B_3	2·56	−5·27	20·17
Final	B_1	2·69	4·80	20·00
	B_2	−5·97	−0·20	20·00
	B_3	2·69	−5·20	20·00

Table 2. Variations of link lengths in Example 1.

Step number	Link lengths					
i	L_1	L_2	L_3	L_4	L_5	L_6
0	18·86	18·82	22·50	22·58	20·90	21·09
1	19·06	19·02	22·34	22·40	20·88	21·07
2	19·25	19·21	22·18	22·22	20·87	21·05
3	19·44	19·41	22·02	22·05	20·86	21·03
4	19·64	19·60	21·86	21·87	20·84	21·01
5	19·83	19·79	21·70	21·69	20·83	20·99
6	20·02	20·00	21·54	21·51	20·82	20·97
7	20·22	20·18	21·38	21·33	20·80	20·95
8	20·41	20·38	21·22	21·15	20·79	20·93
9	20·60	20·57	21·06	20·98	20·78	20·91
10	20·80	20·76	20·89	20·80	20·76	20·89

Table 3. Variations of B co-ordinates and fracture opening in Example 1.

Step number	Co-ordinates			
i	Points	x-Component	y-Component	z-Component
0	B_1	2·51	4·50	18·03
	B_2	−5·67	0·17	21·80
	B_3	2·56	−5·27	20·17
	$\mathbf{KG}'_1$	−2·59	−1·70	0·21
1	B_1	2·55	4·57	18·22
	B_2	−5·74	0·13	21·62
	B_3	2·56	−5·25	20·16
	$\mathbf{KG}'_1$	−2·33	−1·53	0·13
2	B_1	2·58	4·62	18·41
	B_2	−5·80	0·09	21·44
	B_3	2·57	−5·23	20·14
	$\mathbf{KG}'_1$	−2·06	−1·35	0·06
3	B_1	2·61	4·67	18·61
	B_2	−5·85	0·05	21·25
	B_3	2·58	−5·21	20·13
	$\mathbf{KG}'_1$	−1·80	−1·18	0·01
4	B_1	2·64	4·72	18·80
	B_2	−5·89	0·02	21·07
	B_3	2·59	−5·20	20·11
	$\mathbf{KG}'_1$	−1·54	−1·00	−0·03
5	B_1	2·66	4·75	19·00
	B_2	−5·93	−0·02	20·89
	B_3	2·60	−5·19	20·09
	$\mathbf{KG}'_1$	−1·28	−0·83	−0·06
6	B_1	2·67	4·78	19·20
	B_2	−5·95	−0·06	20·71
	B_3	2·61	−5·19	20·08
	$\mathbf{KG}'_1$	−1·02	−0·66	−0·07
7	B_1	2·68	4·79	19·40
	B_2	−5·97	−0·10	20·53
	B_3	2·63	−5·18	20·06
	$\mathbf{KG}'_1$	−0·77	−0·49	−0·07
8	B_1	2·69	4·80	19·60
	B_2	−5·98	−0·13	20·35
	B_3	2·65	−5·19	20·04
	$\mathbf{KG}'_1$	−0·51	−0·33	−0·06
9	B_1	2·69	4·81	19·80
	B_2	−5·98	−0·17	20·18
	B_3	2·67	−5·19	20·02
	$\mathbf{KG}'_1$	−0·25	−0·16	−0·04
10	B_1	2·69	4·80	20·00
	B_2	−5·97	−0·20	20·00
	B_3	2·69	−5·20	20·00
	$\mathbf{KG}'_1$	0·00	0·00	0·00

Table 4. Co-ordinates of points B_1, B_2, B_3 in Example 2.

		Co-ordinates		
Position	Points	x-Component	y-Component	z-Component
Initial	B_1	2·89	5·00	20·00
	B_2	−5·77	0·00	20·00
	B_3	2·89	−5·00	20·00
Final	B_1	3·66	4·07	20·60
	B_2	−5·26	1·32	17·03
	B_3	0·56	−5·38	21·63

After implementation of the theory of Section 2.2, the inverse kinematic results turn out to be the following:

$$c = 8{\cdot}00 \text{ cm};\ L_1 = 20{\cdot}82;\ L_2 = 20{\cdot}82;\ L_3 = 20{\cdot}82;\ L_4 = 20{\cdot}82;\ L_5 = 20{\cdot}82;\ L_6 = 20{\cdot}82.$$
$$L_{1s} = 21{\cdot}10;\ L_{2s} = 21{\cdot}63;\ L_{3s} = 17{\cdot}58;\ L_{4s} = 18{\cdot}32;\ L_{5s} = 21{\cdot}91;\ L_{6s} = 22{\cdot}89.$$

Based on the parameters determined above, a direct kinematic analysis is performed producing the distal ring joint (B_1, B_2, B_3) co-ordinates in Table 4. As can be seen from the figures in Table 4, the initial configuration of the distal ring of the G-S platform fixator is parallel to the proximal one, whereas in the final configuration the distal ring has an oblique position. The numerical results validate the theory of Section 2.2. It means that all the translational and angular deformities present in the initial neutral configuration have been corrected in the final oblique configuration.

If a 10-step treatment strategy is followed by the orthopaedist, then he (or she) should take for the required leg lengths of the G-S platform fixator in each step the values displayed in Table 5.

The direct kinematic analysis results based on the leg lengths of Table 5 are collected in Table 6 for each step. The figures in Table 6 prove that the distal and the proximal bone fragments are orthopaedically reduced after the implementation of the ten-step treatment strategy.

4.3. Example 3

The physical dimensions, the Lateral, AP radiographic data and the clinical examination results are the basic input, while the B-point co-ordinates, as well as the fracture opening are the required output corresponding to the third case.

The Lateral data: $e_y = 3{\cdot}11$ cm; $e_z = 1{\cdot}58$ cm; $b_L = 11{\cdot}61$; $c_L = 7{\cdot}05$ cm; $\beta_L = -6{\cdot}75^\circ$; $\beta'_L = -10{\cdot}35^\circ$.
The AP data: $e_x = -6{\cdot}64$ cm; $\beta_{AP} = 28{\cdot}34^\circ$; $\beta'_{AP} = 15{\cdot}00^\circ$.
The Axial data: $q_x = 0{\cdot}50$ cm; $q_y = 0{\cdot}60$ cm; $r_x = 0{\cdot}70$ cm; $r_y = 0{\cdot}80$ cm; $\delta_0 = 60^\circ$; $\delta_{Ax} = 20{\cdot}00^\circ$.

For the given data taken from the radiographic and the clinical examinations, an inverse kinematic analysis is carried out according to the theory of Section 2.3 and the following results are found:

$$c = 8{\cdot}00 \text{ cm};\ b = 12{\cdot}00 \text{ cm};\ L_1 = 20{\cdot}82;\ L_2 = 20{\cdot}82;\ L_3 = 20{\cdot}82;\ L_4 = 20{\cdot}82;\ L_5 = 20{\cdot}82;$$
$$L_6 = 20{\cdot}82;$$
$$L_{1s} = 19{\cdot}62;\ L_{2s} = 23{\cdot}15;\ L_{3s} = 19{\cdot}14;\ L_{4s} = 18{\cdot}25;\ L_{5s} = 21{\cdot}78;\ L_{6s} = 21{\cdot}55.$$

Table 5. Variations of Link Lengths in Example 2.

Step number	Link lengths					
i	L_1	L_2	L_3	L_4	L_5	L_6
0	20·82	20·82	20·82	20·82	20·82	20·82
1	20·85	20·90	20·49	20·57	20·93	21·02
2	20·87	20·98	20·17	20·32	21·04	21·23
3	20·90	21·06	19·85	20·07	21·14	21·44
4	20·93	21·14	19·52	19·82	21·25	21·65
5	20·96	21·23	19·20	19·57	21·36	21·86
6	20·99	21·31	18·88	19·32	21·47	22·06
7	21·02	21·39	18·55	19·07	21·58	22·27
8	21·05	21·47	18·23	18·82	21·69	22·48
9	21·07	21·55	17·91	18·57	21·80	22·69
10	21·10	21·63	17·58	18·32	21·91	22·89

When the initial and the final leg lengths of the G-S platform fixator are entered into a direct kinematic analysis, it produces the distal ring joint B_1, B_2, B_3 co-ordinates in Table 7.

For a ten-step treatment strategy the calculated leg lengths needed by the orthopaedist to set up the G-S platform fixator at each step are shown in Table 8.

Next, the theory of Section 3 together with the direct kinematic analysis provides the distal ring joint co-ordinates at each step of the treatment strategy displayed in Table 9. It is seen that the bone deformities are totally corrected.

The examples show that by a ten-step treatment strategy, the fracture opening is gradually decreased in magnitude to arrive finally at a zero value, the union configuration. The amounts by which this final target is achieved may be changed if the medical constraints should require this to be so. This is accomplished by simply altering the number of steps. For instance, if the advance size in each step exceeds the medically allowable limit, then the number of intermediate fixation positions can be increased without difficulty. Conditions of the fracture may also impose new constraints on the practicing orthopaedist to vary or plan different trajectories along which the distal fragment end at the fracture site is more conveniently moved. In that case, it may not be sufficient to modify the number of steps only, but the lengths of each link in the fixator may have to be varied unequally according to different experimental or simulation schemes. In this way, the orientation, as well as the magnitude of the linear displacement vector associated with the distal fragment end, will be affected, thus producing many alternative paths out of which the most suitable one can be chosen.

By varying the input data to the theories presented, one may perform numerical experiments to decide on a feasible and most appropriate treatment strategy. However, care should be exercised with the sign convention of the input data. Needless to say that linear quantities are regarded positive when they are measured along the positive directions of any co-ordinate system. It is also tacitly assumed that for the sign of the angular quantities, when viewed against the thumb or axis direction, the right-hand rule determines the positive sense, *i.e.*, counter-clockwise being (+).

Table 6. Variations of B co-ordinates and fracture opening in Example 2.

Step number		Co-ordinates		
i	Points	*x*-Component	*y*-Component	*z*-Component
0	B_1	2·89	5·00	20·00
	B_2	−5·77	0·00	20·00
	B_3	2·89	−5·00	20·00
	$\mathbf{KG}'_1$	−3·58	1·03	0·10
1	B_1	2·97	4·92	20·06
	B_2	−5·82	0·15	19·69
	B_3	2·69	−5·08	20·17
	$\mathbf{KG}'_1$	−3·24	1·02	0·81
2	B_1	3·05	4·83	20·12
	B_2	−5·84	0·30	19·39
	B_3	2·50	−5·15	20·33
	$\mathbf{KG}'_1$	−2·90	0·10	0·65
3	B_1	3·12	4·74	20·18
	B_2	−5·84	0·44	19·09
	B_3	2·29	−5·22	20·50
	$\mathbf{KG}'_1$	−2·55	0·95	0·50
4	B_1	3·20	4·65	20·25
	B_2	−5·81	0·58	18·79
	B_3	2·07	−5·28	20·67
	$\mathbf{KG}'_1$	−2·19	0·88	0·37
5	B_1	3·28	4·56	20·31
	B_2	−5·77	0·71	18·49
	B_3	1·85	−5·33	20·83
	$\mathbf{KG}'_1$	−1·83	0·79	0·26
6	B_1	3·36	4·46	20·37
	B_2	−5·71	0·84	18·19
	B_3	1·62	−5·37	20·99
	$\mathbf{KG}'_1$	−1·46	0·67	0·17
7	B_1	3·43	4·37	20·42
	B_2	−5·63	0·97	17·90
	B_3	1·37	−5·39	21·15
	$\mathbf{KG}'_1$	−1·10	0·54	0·10
8	B_1	3·51	4·27	20·48
	B_2	−5·52	1·09	17·61
	B_3	1·12	−5·41	21·32
	$\mathbf{KG}'_1$	−0·73	0·38	0·05
9	B_1	3·59	4·17	20·54
	B_2	−5·40	1·20	17·32
	B_3	0·85	−5·40	21·48
	$\mathbf{KG}'_1$	−0·25	−0·16	−0·04
10	B_1	3·66	4·07	20·60
	B_2	−5·26	1·32	17·03
	B_3	0·56	−5·38	21·63
	$\mathbf{KG}'_1$	0·00	0·00	0·00

Table 7. Co-ordinates of points B_1, B_2, B_3 in Example 3.

		Co-ordinates		
Position	Points	x-Component	y-Component	z-Component
Initial	B_1	2·89	5·00	20·00
	B_2	−5·77	0·00	20·00
	B_3	2·89	−5·00	20·00
Final	B_1	8·96	0·44	19·36
	B_2	−0·69	−1·65	17·81
	B_3	5·81	−9·04	19·56

Table 8. Variations of link lengths in Example 3.

Step number	Link lengths					
i	L_1	L_2	L_3	L_4	L_5	L_6
0	20·82	20·82	20·82	20·82	20·82	20·82
1	20·70	21·05	20·65	20·56	20·91	20·89
2	20·58	21·28	20·48	20·30	21·01	20·96
3	20·46	21·52	20·31	20·05	21·11	21·04
4	20·34	21·75	20·14	19·79	21·20	21·11
5	20·22	21·98	19·98	19·53	21·30	21·18
6	20·10	22·22	19·81	19·28	21·40	21·26
7	19·98	22·45	19·64	19·02	21·49	21·33
8	19·86	22·68	19·47	18·77	21·59	21·40
9	19·74	22·92	19·30	18·51	21·69	21·48
10	19·62	23·15	19·14	18·25	21·78	21·55

5. Conclusions

In this work theories have been presented as to how a 3-3 type G-S Platform Mechanism can be utilized to form medically amenable treatment strategies under miscellaneous cases of extremity fractures and deformity-correction processes. The different theories are based on the coupling of the medical input data, such as those obtained from radiographic and clinical measurements with the inverse and forward kinematics of the fixator assembly. They have been tested on numerical examples to provide verification. Results have demonstrated that, by varying the input, miscellaneous alternatives can be developed to fit to the orthopaedists' needs for an effective treatment strategy.

This work has been basically founded on three related scenarios. In the first scenario, the proximal and distal bone fragments are attached perpendicular to the base and moving planes of the G-S platform mechanism, respectively, to form a 6 degree-of-freedom spatial external fixator. Depending on the radiographic and clinical data, the lengths of the bars joining the proximal ring to the distal ring are calculated by performing an inverse kinematic analysis, both at the initial and final configuration of the G-S platform. If the entered data represent accurate measurements, then the misaligned bone fragments are brought to their anatomically

Table 9. Variations of B co-ordinates and fracture opening in Example 3.

Step number	Co-ordinates			
i	Points	*x*-Component	*y*-Component	*z*-Component
0	B_1	2·89	5·00	20·00
	B_2	−5·77	0·00	20·00
	B_3	2·89	−5·00	20·00
	$\mathbf{KG}'_1$	−6·64	3·11	1·58
1	B_1	3·48	4·56	20·06
	B_2	−5·32	−0·18	19·84
	B_3	3·19	−5·43	20·01
	$\mathbf{KG}'_1$	−5·97	2·88	1·49
2	B_1	4·08	4·12	20·09
	B_2	−4·85	−0·36	19·67
	B_3	3·50	−5·86	20·00
	$\mathbf{KG}'_1$	−5·31	2·64	1·39
3	B_1	4·68	3·67	20·10
	B_2	−4·37	−0·53	19·49
	B_3	3·80	−6·29	19·98
	$\mathbf{KG}'_1$	−4·65	2·37	1·27
4	B_1	5·29	3·22	20·08
	B_2	−3·87	−0·71	19·29
	B_3	4·10	−6·70	19·95
	$\mathbf{KG}'_1$	−3·98	2·09	1·14
5	B_1	5·89	2·77	20·03
	B_2	−3·37	−0·87	19·09
	B_3	4·40	−7·12	19·90
	$\mathbf{KG}'_1$	−3·32	1·80	1·00
6	B_1	6·50	2·31	19·95
	B_2	−2·86	−1·04	18·87
	B_3	4·69	−7·52	19·85
	$\mathbf{KG}'_1$	−2·65	1·48	0·84
7	B_1	7·11	1·85	19·85
	B_2	−2·33	−1·19	18·63
	B_3	4·98	−7·92	18·79
	$\mathbf{KG}'_1$	−1·99	1·14	0·66
8	B_1	7·73	1·38	19·72
	B_2	−1·80	−1·35	18·37
	B_3	5·26	−8·31	19·72
	$\mathbf{KG}'_1$	−1·32	0·79	0·46
9	B_1	8·34	0·92	19·55
	B_2	−1·25	−1·50	18·10
	B_3	5·54	−8·68	19·64
	$\mathbf{KG}'_1$	−0·66	0·41	0·24
10	B_1	8·96	0·44	19·36
	B_2	−0·69	−1·65	17·81
	B_3	5·81	−9·04	19·56
	$\mathbf{KG}'_1$	0·00	0·00	0·00

correct positions in the final configuration of the fixator, whereby the proximal and distal rings are parallel to each other

For many reasons like the entry of inaccurate data, violation of assumptions, geometric irregularities in the bones or residual deformities, the bone fragments may turn out to be unreduced at the end of the treatment process, *i.e.*, when the neutral configuration is reached in the first scenario. In that case, a second treatment phase is to be initiated from the neutral configuration to ultimately end up with a union configuration at the fracture site. In another situation, fracture conditions may require the fixing of the distal bone fragment to the moving plane of the G-S platform at an oblique position when the base and moving platforms are initially parallel. This constitutes the second scenario, in which a new inverse kinematic analysis is carried out to calculate the leg lengths of the fixator corresponding to a new set of radiographic and clinical measurements in both the initial and final configurations.

The third scenario arises when, after the application of the first scenario, the radiographic and clinical examinations point to a wrong fixation of the bones to their respective rings. It may also be generated out of a situation whereby the fractured bone conditions dictate that both the distal and proximal bone fragments be fixed to the moving and base planes of the G-S platform mechanism, respectively, at different oblique positions. In those cases, new leg lengths have to be calculated that correspond to the correct radiographic and clinical data. When the translational and rotational misalignments have been removed from the broken parts of the extremity, the moving platform takes on an oblique position relative to the base.

It is of the utmost importance for the orthopaedic surgeon to know the proper values of the bar lengths of the G-S platform mechanism in order to set up the spatial fixator as envisaged. On the other hand, he (or she) may wish to see how closer the two ends of the bone fragments are moved with respect to each other during the course of healing for a desirable union configuration. To that end, a direct analysis has been performed in the work leading to the generated trajectory of the distal bone end as viewed from the base. There might be a number of possibilities for the orthopaedist to change the trajectory by picking up several feasible leg lengths between their initial and final values.

Thanks to the existence of closed loops within its kinematic structure, the G-S platform mechanism provides a limited but adequate workspace, as well as a stiff parallel robotic structure for the orthopaedic applications as a suitable spatial external fixator. Bar lengths, being fundamental kinematic parameters, will affect both the workspace and the stiffness of the fixator significantly. If more stiffness is required on the part of bone fragments at the union configuration, this is to be secured possibly by shorter bar lengths. Thus, from such a point of view, the first scenario appears to be the most preferable one to be implemented by the orthopaedic surgeon, when there is room for such a choice. Whether the optimum stiffness demanded by the treatment process matches with the neutral configuration is a hypothesis to be substantiated by further research.

In case the surgeon could describe the trajectory along which the distal bone end could be moved most conveniently to bring it in complete alignment with the proximal bone end, then it should be possible to set up a procedure for the evaluation of necessary bar lengths for that purpose. In this work, bones are only represented by their mid-points. However, if they are badly deformed to the extent that they can no longer be represented as cylinders, then points outside their axes might have to be taken into consideration as well. In such cases, the work can be extended to cover these points.

Appendix A: Derivation of Equation (1–4):

A rectangular prism with the sides C_x, C_y, C_z along the axes *x, y, z* of an orthogonal reference system is shown in Figure 5. The axis (w) of a rod having length c coincides with the diagonal of the prisms as seen in Figure 5. If the angles measured between the projections of the rod onto the zx, zy and yx-planes and the corresponding z, z, y-axes are denoted by β_{AP}, β_L, β_{Ax}, respectively, as shown in Figure 5, then the following relationships can be written:

$$C_x = C_L \cos\beta_L \tan\beta_{AP}; \quad C_y = C_L \sin\beta_L; \quad C_z = C_L \cos\beta_L, \tag{A-1}$$

where C_L is the length of the projected rod in the yz-plane. Now, in the light of the relationships (A-1), Equations (1–4) can be obtained by successive substitutions among the following relationships written from Figure 5:

$$\tan\beta_{Ax} = \frac{C_x}{C_y}; \quad \tan\beta_{wz} = \frac{C_x}{C_z \sin\beta_{Ax}}, \tag{A-2}$$

$$\tan\beta_{wy} = \frac{\sqrt{C_z^2 + C_x^2}}{C_y}; \quad \tan\beta_{wx} = \frac{\sqrt{C_y^2 + C_z^2}}{C_x}, \tag{A-3}$$

where β_{wx}, β_{wy}, β_{wz} are direction cosine angles of the axis w in the Oxyz-reference system.

Appendix B: Derivation of Equations (22–23):

The distal triangle $B_1B_2B_3$ is drawn in Figure 6. Given the sides b_1, b_2, b_3 of the triangle, the angles $\varphi_1, \varphi_2, \varphi_3$ can be determined by the application of the cosine law, leading to the equation set (23). Since points B_1, B_2, B_3 are on a circle with center at G_1 and with radius R_1, it follows that the triangles $B_1G_1B_2$, $B_2G_1B_3$, $B_3G_1B_1$ are isosceles triangles. Hence, the following equations are written from Figure 6:

$$\delta_3 + \delta_1 = \varphi_1, \quad \delta_1 + \delta_2 = \varphi_2, \quad \delta_2 + \delta_3 = \varphi_3. \tag{B-1}$$

The solution of (B-1) for δ_1, δ_3 yields (22).

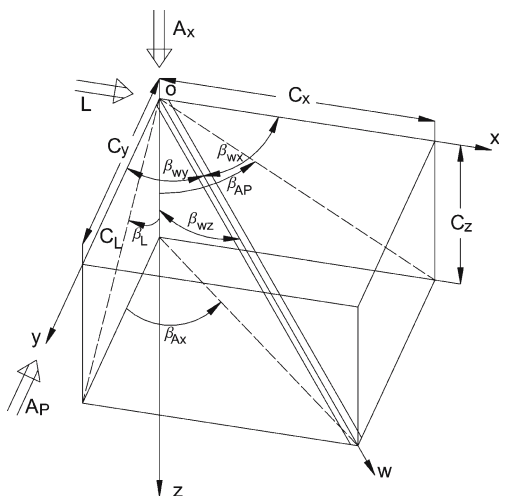

Figure 5. Projections of a rod with w axis in the Oxyz-system.

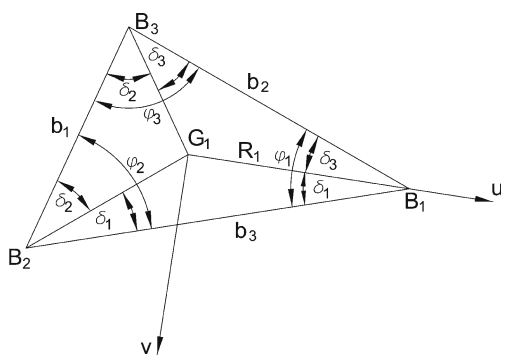

Figure 6. The distal triangle.

Appendix C: Derivation of Equations (59–64):

The following solution procedure is applied to arrive at Equations (59–64). First, subtract (16) from (17) and from (18) side by side to yield the following:

$$\mathbf{GB}_k - \mathbf{GB}_1 = \mathbf{G}_1\mathbf{B}_k - \mathbf{G}_1\mathbf{B}_1, \quad k = 2, 3. \tag{C-1}$$

Then substitute $\mathbf{G}_1\mathbf{B}_k$ $k = 2, 3$ from Equations (19–21) in (C-1) to get two vector equations with two vector unknowns $\mathbf{e}_u$, $\mathbf{e}_v$. Note that, since by direct kinematics the point B_i $i = 1, 2, 3$ co-ordinates (B_{ix}, B_{iy}, B_{iz}) have been determined in the fixed Gxyz co-ordinate system for a given set of leg lengths, the unit vectors $\mathbf{e}_u$, $\mathbf{e}_v$ are solved from the linear equation (C-1) in terms of the unit vectors **i, j, k** defined in the fixed Gxyz-system. Now that $\mathbf{e}_u$,$\mathbf{e}_v$ have been expressed in the **i, j, k** unit vectors, the co-ordinates (g_{1x}, g_{1y}, g_{1z}) of the point G_1 are now obtained from one of the Equations (16–18). After lengthy algebraic manipulations accompanied by trigonometric identities, the formulas (58–63) are obtained. Equation (64) follows from $\mathbf{e}_w = \mathbf{e}_u \mathrm{x} \mathbf{e}_v$, (*i.e.*, $\mathbf{e}_w$ is the cross-product of the vectors $\mathbf{e}_u$, $\mathbf{e}_v$) based on the orthogonality of axes according to the right-hand rule.

Appendix D: List of symbols

A_1, A_2, A_3	Spherical joint points on base platform.
a_1, a_2, a_3	Side lengths of the proximal triangle.
$[A_{Gxyz}^{G_1uvw}]$	Rotation matrix of the moving co-ordinate system relative to the fixed co-ordinate system.
$[A_{Gxyz}^{G_1uvw}]_1$	Rotation matrix at the initial configuration.
$[A_{Gxyz}^{G_1uvw}]_2$	Rotation matrix at the final configuration.
$[A_{G_1''u'v'w'}^{G_1uvw}]_1$	Relative rotation matrix at the initial configuration.
$[A_{Gxyz}^{Gx'y'z'}]$	Relative rotation matrix associated with the proximal fragment.
AP	Antero-posterior
B_1, B_2, B_3	Spherical joint points on moving platform.
b, c	The fragment lengths on the proximal and distal sides, respectively.
b_1, b_2, b_3	Side lengths of the distal triangle.
b_L, c_L	The projected lengths of the proximal and distal fragments on the lateral plane.
C_x, C_y, C_z	Sides of a rectangular prism along x,y,z-axes of an orthogonal reference system.
$\mathbf{e}_u$, $\mathbf{e}_v$, $\mathbf{e}_w$	The unit vectors of the moving co-ordinate system.
e_{ux}, e_{uy}, e_{uz}	Components of the $\mathbf{e}_u$ unit vector along the fixed x,y,z-axes.
e_{vx}, e_{vy}, e_{vz}	Components of the $\mathbf{e}_v$ unit vector along the fixed x,y,z-axes.
e_{wx}, e_{wy}, e_{wz}	Components of the $\mathbf{e}_w$ unit vector along the fixed x,y,z-axes.
$[\mathbf{e}_{u'}\mathbf{e}_{v'}\mathbf{e}_{w'}]$	Unit vectors of the moving reference system attached to the distal bone center.
$e_{u'x}$, $e_{u'y}$, $e_{u'z}$	The $\mathbf{e}_{u'}$ unit vector components of the moving reference system attached to the distal bone center.
$e_{v'x}$, $e_{v'y}$, $e_{v'z}$	The $\mathbf{e}_{v'}$ unit vector components of the moving reference system attached to the distal bone centre.
$e_{w'x}$, $e_{w'y}$, $e_{w'z}$	The $\mathbf{e}_{w'}$ unit vector components of the moving reference system attached to the distal bone centre.

e_x, e_y, e_z	Relative translations of the fragment bone ends along *x,y,z*-axes, respectively.
$\mathbf{e}_{x'}$ $\mathbf{e}_{y'}$ $\mathbf{e}_{z'}$	Unit vectors of the reference system fixed to the proximal bone center.
G	Proximal ring center.
G′	Proximal bone center.
G_1	Distal ring center.
G_1'	Distal bone end.
G_1''	Distal bone center.
$\mathbf{GA}_1$, $\mathbf{GA}_2$, $\mathbf{GA}_3$	Position vectors of spherical joint points on base platform relative to fixed co-ordinate system.
$\mathbf{G_1B}_1$, $\mathbf{G_1B}_2$ $\mathbf{G_1B}_3$	Position vectors of spherical joint points on moving platform relative to moving co-ordinate system.
$\mathbf{GB}_1$, $\mathbf{GB}_2$, $\mathbf{GB}_3$	Position vectors of spherical joint points on moving platform relative to fixed co-ordinate system.
$\mathbf{GB}_{1s}$, $\mathbf{GB}_{2s}$, $\mathbf{GB}_{3s}$	Position vectors of spherical joint points on moving platform relative to fixed co-ordinate system for the final configuration.
$\mathbf{GG}_1$	Position vectors of the distal ring center.
$\mathbf{G_1G}_1''$	Position vector of intersection of the distal bone axis and distal ring plane relative to the distal ring center.
$\mathbf{G}_1'\mathbf{G}_1''$	Position vector of intersection of the distal bone axis and distal ring plane relative to the distal bone end.
GK	Position vector of the proximal bone end.
G_1uvw	Moving co-ordinate system fixed to the distal ring center.
$G_1''u'v'w'$	Moving co-ordinate system fixed to the distal bone center.
Gxyz	Co-ordinate system fixed to the proximal ring center.
$G'x'y'z'$	Co-ordinate system fixed to the proximal bone center.
g_{1x}, g_{1y}, g_{1z}	The co-ordinates of the distal ring center in the fixed system.
h	Distance between the proximal and distal ring planes along z-direction at neutral position.
h_0	The initial height between the base and moving platforms along the z-axis.
i, j, k	Unit vectors of the fixed system.
i, j, k	Indices.
K	Proximal bone end.
$\mathbf{KG}_1'$	Position vector of the distal bone end relative to the proximal bone end.
L	Lateral
(L_1-L_6)	Leg lengths of the G-S Platform Mechanism.
L_{1s},L_{2s},L_{3s}, L_{4s},L_{5s},L_{6s}	Leg lengths of the G-S Platform Mechanism for the final configuration.
n	Number of steps in a treatment strategy.
q_x, q_y	The distances between the centers of the proximal ring and the proximal fragment along x,y directions in the proximal ring plane, respectively.
R	Proximal ring radius.
R_1	Distal ring radius.
rot [γ, η, α]	Rotation matrix involving γ, η, α rotations about x, y, z-axes, respectively.
r_u, r_v,	The distances between the centers of the distal ring and distal fragment along the directions in the moving ring plane, respectively.

r_x, r_y, r_z	The distances between the centers of the distal ring and distal fragment along x,y,z directions, respectively, in the fixed Gxyz-system.
β_1, β_2, β_3	Angles of the proximal isosceles triangles.
β_{Ax}	The projected angle of the w-axis in the axial direction.
β_L, β_{AP}	The angles measured between the vertical z-axis and projected axes of the distal fragment on the lateral (L) and on the AP planes, respectively.
β_{wx}, β_{wy}, β_{wz}	The angles between the w-axis of the moving and the fixed axes of the base co-ordinate systems, respectively.
$\beta_{z'x}$, $\beta_{z'y}$, $\beta_{z'z}$	Direction cosine angles of the z'-axis.
β'_{Ax}	The projected angle of the z'-axis in the axial direction.
β'_L, β'_{AP}	The angles measured between the vertical z-axis and the projected axis of the proximal fragment on the lateral (L) and on the AP planes, respectively.
δ_0	The relative rotation of the distal ring with respect to the proximal ring.
$\delta_1, \delta_2, \delta_3$	Angles of the distal isosceles triangles.
δ_{Ax}	The projected relative angular displacement of the distal fragment with respect to the proxiaml fragment in the axial view.
ϕ_1, ϕ_2, ϕ_3	Angles of the proximal triangle.
$\varphi_1, \varphi_2, \varphi_3$	Angles of the distal triangle.
γ, η, α	Angles of rotation about x, y and z-axes, respectively.
γ', η', α'	Angles of rotation about x', y' and z'-axes, respectively.
ΔL	Leg length difference between the initial and final configurations of the GS
ΔS	Link length increment or decrement.

References

1. G. Ilizarov, *Transosseons Osteonsynthesis*. Berlin: Springer Verlag (1992) 800 pp.
2. D. Paley, *Principles of Deformity Correction.* Berlin: Springer Verlag (2002) 806 pp.
3. J.C. Taylor, Correction of general deformity with the Taylor spatial frame fixator. *www.jcharlestaylor.com* (1996).
4. V.E. Gough and S.G. Whitehall, Universal tire test machine. *Proc. of the 9th International Technical Congress*. F.I.S.I.T.A. Inst. Mech. E. (1962) p. 177.
5. D. Stewart, A platform with six degrees of freedom. *Proc. of I. Mech. E* 180 (1965) 371–386.
6. I.D. Akcali and H. Mutlu, A novel approach in the direct kinematics of Stewart platform mechanisms with planar platforms. *ASME J. Mech. Design* 127 (2005) 1–12.
7. C. Innocenti and V. Parenti-Castelli, Direct position analysis of the Stewart platform mechanism. *Mech. Mach. Theory* 25 (1990) 611–621.
8. C. Liang, L. Han and F. Wen, Forward displacement analysis of the 5-6 Stewart platforms. *Proc. of the 9th World Congress on TMM* (1995) pp. 184–187.
9. D.M. Ku, Direct displacement analysis of a Stewart platform mechanism. *Mech. Mach. Theory* 34 (1999) 453–465.
10. T.Y. Lee and J.K. Shim, Forward kinematics of the general 6-6 Stewart platform using algebraic elimination. *Mech. Mach. Theory* 36 (2001) 1073–1085.
11. M. Griffis and J. Duffy, A forward displacement analysis of a class of Stewart platforms. *J. Robot. Syst.* 6 (1989) 703–720.
12. I. Hostens, J. Anthonis and H. Raman, New design for a 6 dof vibration simulator with improved reliability and performance. *Mech. Syst. Signal Proc.* 19 (2005) 105–122.
13. K.C. Fan, H. Wang, J.W. Zhao and T.H. Change, Sensitivity analysis of the 3-PRS parallel spindle platform of a serial-parallel machine tool. *Int. J. Machine Tools Manuf.* 43 (2003) 1561–1569.
14. J.J. Craig, *Introduction to Robotics Mechanics & Control.* Reading: Addison-Wesley (1989) 303 pp.
15. K.S. Fu, R.C. Gonzales and C.S.G. Lee, *Robotics: Control, Sensing, Vision and Intelligence.* New York: McGraw-Hill (1987) 580 pp.